Tkac, O., Orr-Ewing, A. J., Dagdigian, P. J., Alexander, M. H., Onvlee, J., & van der Avoird, A. (2014). Collision dynamics of symmetric top molecules: A comparison of the rotationally inelastic scattering of CD3 and ND3 with He. *Journal of Chemical Physics*, *140*(13), [134308]. https://doi.org/10.1063/1.4869596

Collision dynamics of symmetric top molecules: A comparison of the rotationally inelastic scattering of CD_3 and ND_3 with He

Ondřej Tkáč,[1] Andrew J. Orr-Ewing,[1] Paul J. Dagdigian,[2,a)] Millard H. Alexander,[3] Jolijn Onvlee,[4] and Ad van der Avoird[4,b)]

[1)] *School of Chemistry, University of Bristol, Cantock's Close, Bristol BS8 1TS, UK*
[2)] *Department of Chemistry, The Johns Hopkins University, Baltimore, Maryland 21218-2685, USA*
[3)] *Department of Chemistry and Biochemistry and Institute for Physical Science and Technology, University of Maryland, College Park, Maryland 20742-2021, USA*
[4)] *Radboud University Nijmegen, Institute for Molecules and Materials, Toernooiveld 1, 6525ED Nijmegen, The Netherlands*

[a)]Electronic mail: pjdagdigian@jhu.edu
[b)]Electronic mail: avda@theochem.ru.nl

Abstract

We compare rotationally inelastic scattering of deuterated methyl radicals (CD_3) and ammonia (ND_3) in collisions with helium using full close-coupling quantum-mechanical scattering calculations performed with ab initio potential energy surfaces (PESs). The theoretical methods have been rigorously tested against angle-resolved experimental measurements obtained using crossed molecular beam apparatuses in combination with velocity map imaging [O. Tkáč *et al.*, Chem. Sci. **4**, 4199 (2013); O. Tkáč *et al.*, Phys. Chem. Chem. Phys. **16**, 477 (2014)]. Common features of the scattering dynamics of these two symmetric top molecules, one closed-shell and the other an open-shell radical, are identified and discussed. Two types of anisotropies in the PES influence the interaction of an atom with a nonlinear polyatomic molecule. The effects of these anisotropies can be clearly seen in the state-to-state integral cross sections out of the lowest CD_3 rotational levels of each nuclear spin symmetry at a collision energy of 440 cm^{-1}. Similarities and differences in the differential cross sections for the ND_3–He and CD_3–He systems can be linked to the coupling terms derived from the PESs which govern particular initial to final rotational level transitions.

I. Introduction

In recent experiments from our laboratories, the rotationally inelastic scattering dynamics of symmetric top molecules in collisions with rare gas atoms were examined using crossed molecular beam and velocity map imaging (VMI) methods and compared with quantum scattering calculations.[1,2] The bulk of experimental and theoretical studies of the dynamics of rotational energy transfer involved studies of collisions of diatomic molecules, as exemplified by a number of recent studies.[3-10] Similar attention has also been paid to experimental and theoretical studies of inelastic collisions of nonlinear polyatomic molecules.[11-21] Collisions of nonlinear polyatomic molecules, such as the symmetric tops under study here, display a richer dynamics because the potential energy surface (PES) depends upon two angular coordinates, rather than just one as for diatomics, and the energy level structure is more complicated. In particular, there are two types of anisotropies for the interaction of a symmetric top molecule with a structureless collision partner, involving approach of the perturber along and perpendicular to the molecular symmetry axis. By contrast, the anisotropy in an atom-diatom interaction only involves differences between end-on vs. side-on approach. In a recent review article, Dagdigian[22] discussed the effect of the two types of anisotropies in the PES for inelastic collisions of small hydrocarbon reactive intermediates.

The particular symmetric tops selected for investigation here are deuterated methyl (CD_3) and ammonia (ND_3) molecules, and we will focus on collisions with helium. In our experimental studies of these molecules,[1,2] resonance-enhanced multi-photon ionization detection (REMPI) allowed acquisition of VMI for methyl radicals in levels corresponding to a single rotational angular momentum quantum number n', but averaged over a subset of the projection quantum number k', whereas for ND_3, images were acquired for molecules scattered into individual $n'^{\pm}_{k'}$ levels. Product rotational level resolved angular scattering distributions for the CD_3–He and ND_3–He systems were extracted from the experimental images and were compared with the results of full close-coupling quantum-mechanical scattering calculations that used recently developed *ab initio* PESs. The experimental measurements provided rigorous tests of the accuracy of the PESs and computed quantum scattering dynamics, and agreement between experiment and theory was found to be excellent for both the CD_3–He and ND_3–He systems.

The aim of the current paper is to compare the rotationally inelastic scattering dynamics of these two symmetric top molecules, one a closed-shell molecule (ND_3) and the other an open-shell radical (CD_3) and to relate any differences to specific features of the PESs for the two

systems. Although our velocity map imaging (VMI) study of ND_3–He scattering was fully resolved in the pre- and post-collision rotational levels of the ND_3, precise comparisons with CD_3–He scattering based solely on experimental results are difficult because the REMPI detection scheme for CD_3 was not fully k' level specific for a given n'. Moreover, the initial population of n and k levels in the photolytically generated and supersonically cooled beam of CD_3 radicals was distributed over a few different rotational levels. However, our detailed comparison of experimental and theoretical scattering dynamics demonstrated that the quantum scattering calculations provided an accurate description of the collision dynamics for both ND_3–He and CD_3–He. Therefore, we focus here on a comparison between the computational results for these two systems, but recognize that these comparisons are underpinned by the validation provided by our experimental measurements.

This paper is organized as follows. In Sec. II we review the rotational level structures of the two symmetric tops of interest, with consideration of the effects of deuterium nuclear spin, discuss the ND_3–He and CD_3–He PESs, and describe briefly the quantum scattering calculations. Section III presents the calculated integral and differential cross sections for the two systems and discusses the observed propensities for certain types of transitions in terms of the anisotropies of the PESs. A Conclusion follows.

II. Method

A. Rotational levels of ND_3 and CD_3

The three-fold rotational symmetry of the symmetric top molecules, the symmetry / asymmetry of their vibrational wave functions associated with umbrella inversion, and the nuclear spin symmetry types of the three equivalent deuterium atoms all influence the inelastic scattering dynamics in collisions with a rare gas atom. In this subsection, we briefly describe the rotational levels of the CD_3 and ND_3 molecules and their nuclear spin symmetries. Rotational level diagrams for CD_3 and ND_3 are shown in Fig. 1 for the ground vibrational level of their $\tilde{X}$ electronic states. Both molecules are symmetric tops, and we designate the rotational levels by n_k, where n and k (taken to be nonnegative) designate, respectively, the rotational quantum number and its body-frame projection. Rotational levels with $k > 0$ are doubly degenerate.

Ammonia in the ground electronic state has a pyramidal (C_{3v}) equilibrium geometry.[23] The double-minimum potential along the inversion coordinate associated with the ν_2 "umbrella" vibrational mode of ammonia gives rise to a splitting of all rotational levels into levels that are

symmetric and antisymmetric (denoted by + and –, respectively) with respect to the umbrella coordinate. The ground state inversion tunnelling splitting for $n_k = 0_0$ in ND_3 is 0.0530 cm^{-1}.[24,25] The ground electronic state of methyl has a planar (D_{3h}) equilibrium geometry,[26] and there is no inversion splitting in this radical.

Because the three D atoms, with nuclear spin $I = 1$, are equivalent, the ground vibronic states of CD_3 and ND_3 have three nuclear spin modifications. CD_3 rotational levels have the following nuclear spin symmetries: the A_1 nuclear spin functions are those with rotational levels with $k = 0$ and odd n and levels for which k is a multiple of 3; the A_2 nuclear spin functions correspond to rotational levels with even n and $k = 0$ and levels for which k is a multiple of 3; and the E nuclear spin functions include all levels for which k is not a multiple of 3. Thus, CD_3 rotational levels with $k = 3, 6, \ldots$ have two components, A_1 and A_2. Because of the inversion doubling, there are ND_3 levels of both A_1 and A_2 symmetry for each value of n in the $k = 0$ manifold. For this manifold, the + inversion levels for even and odd n have A_1 and A_2

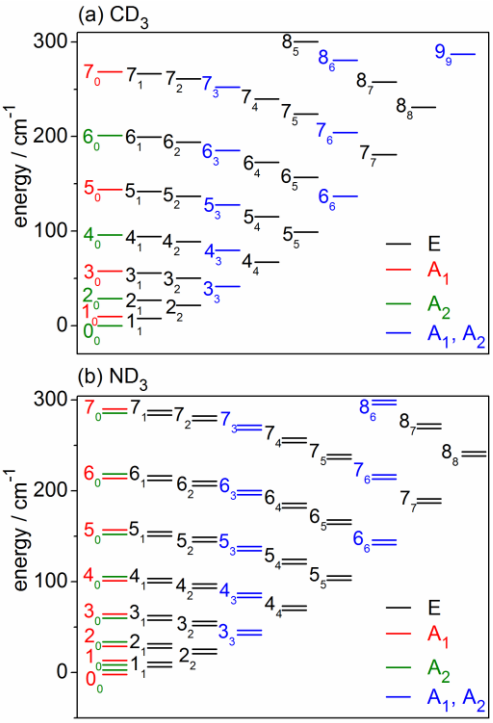

FIG. 1. Rotational energy level diagrams for the ground vibrational levels of the $\tilde{X}$ electronic state of (a) CD_3 and (b) ND_3. Levels are labelled by n_k rotational quantum numbers. The color coding identifies the different nuclear spin modifications. The lower and upper levels in each doublet of ND_3 correspond to the + and – symmetries of the umbrella vibrational wave functions. The inversion splitting is exaggerated for clarity.

symmetry, respectively, while the – inversion levels for odd and even n have A_1 and A_2 symmetry. There are both A_1 and A_2 levels for levels where k is a multiple of 3. As with CD_3, the ND_3 E nuclear spin functions include all levels for which k is not a multiple of 3. The CD_3 and ND_3 nuclear spin modifications do not interconvert between different nuclear spin modifications during collisions.

B. Potential energy surfaces for CD_3–He and ND_3–He

The PESs employed in the scattering calculations were computed with coupled-cluster methods. Details of these quantum mechanical calculations can be found in the literature.[27,28] A CH_3–He PES was computed with CH_3 fixed at its equilibrium geometry. Since the centre-of-mass of methyl is located at the carbon atom, this PES could be used without modification for the CD_3 isotopologue. In subsequent work, we computed a PES for which the CD_3 geometry was averaged over the probability distribution for the ν_2 umbrella coordinate.[29] The interaction was expanded in terms of spherical harmonics as[30]

$$V(R,\theta,\phi) = \sum_{\lambda,\mu\geq 0} V_{\lambda\mu}(R)(1+\delta_{\mu 0})^{-1}[Y_{\lambda\mu}(\theta,\phi) + (-1)^{\mu} Y_{\lambda,-\mu}(\theta,\phi)] \qquad (1)$$

The potential energy depends on the atom-molecule separation R and the orientation of the perturber, given by the angles θ (polar angle from the C_3 symmetry axis) and ϕ (azimuthal angle from a C–D bond) of the He atom with respect to the centre-of-mass of the molecule [see Fig. 1 of Ref. 27].

The ND_3–He PES was obtained from the PES computed by Gubbels *et al.*[28] for NH_3–He. This PES was computed as a function of four coordinates: R, θ, ϕ, and ρ. Here, ρ is the umbrella or inversion angle, defined as the angle between the C_3 axis and a vector pointing from the N atom to one of the H atoms, so $\rho = \pi/2$ corresponds to a planar ND_3 geometry. Also, $\theta = 0°$ corresponds to approach of the He atom toward the lone pair on ammonia. The ND_3 and NH_3 isotopologues have the same electronic structure, and we assume also the same bond lengths; hence, the NH_3–He and ND_3–He interaction potentials are identical. However, the monomer centre-of-mass shifts along the C_3 axis of the molecule, and the R and θ Jacobi coordinates are shifted (the azimuthal angle ϕ and the ρ inversion coordinate are unaffected by isotopic substitution). Hence, a new angular expansion of the PES was carried out for the ND_3–He system.[2] The ND_3–He PES was expanded slightly differently from the angular expansion for the CD_3–He PES. In particular, the former was expanded in terms of tesseral spherical harmonics

$S\lambda\mu(\theta,\phi)$,[28,31] and the origin of the azimuthal angle ϕ was chosen to lie between two N–D bonds and so was 60° different from that for the CD_3–He PES. Therefore, the expansion coefficients for ND_3–He were rescaled for comparison with corresponding CD_3–He coefficients.

The ammonia inversion motion in the ND_3–He scattering calculations was included by the use of a two-state model.[11,28] In this model the $v_2 = 0$ inversion tunneling levels of ammonia are approximated as an even and odd combination of the two rigid equilibrium structures. The ρ dependence of the intermolecular potential is not employed in this method, only the potential for the equilibrium umbrella angle ρ_e.

Contour plots of the CD_3–He and ND_3–He PESs as a function of the angular coordinates θ and ϕ for two atom-molecule separations R are presented in Fig. 2. At the smaller values of R the interaction energies span the collision energies of the molecular beam experiments,[1,2] while the larger R values are close to those of the respective global minima. At the global minimum of the PESs the He atom is located at $\theta = 90°$ (in the molecular plane in case of CD_3) and bisecting the D–C/N–D angle. The atom-molecule separations at the global minima are 6.52 and 6.095

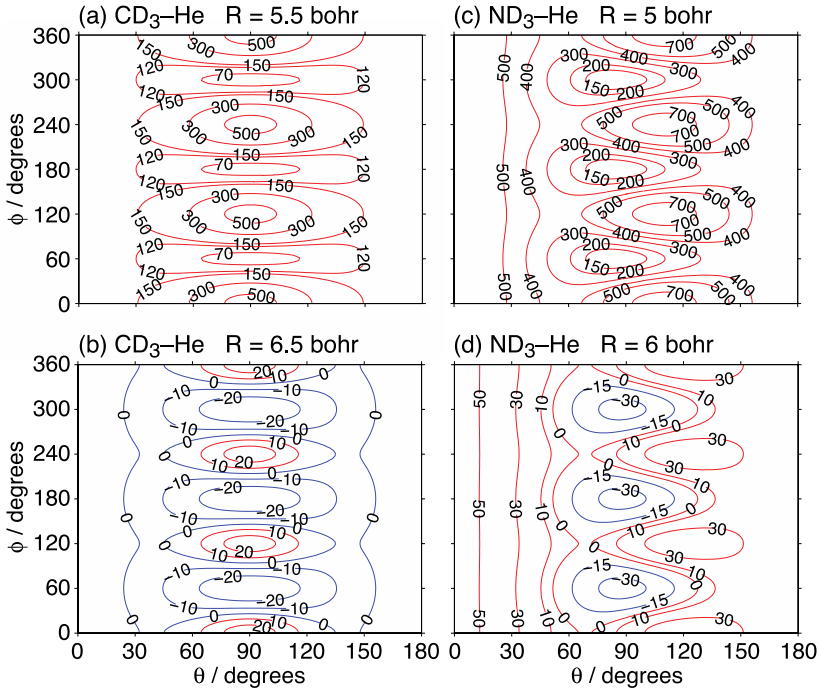

FIG. 2. Dependence of the interaction energy (in cm^{-1}) of the CD_3–He and ND_3–He systems on the orientation of the He atom with respect to the molecule at atom-molecule separations R of (a) 5.5 and (b) 6.5 bohr for CD_3–He and (c) 5 and (d) 6 bohr for ND_3–He.

bohr, and the dissociation energies are 27 and 35 cm^{-1} for CD_3–He and ND_3–He PES, respectively.[27,28] The ϕ angle for the ND_3–He PES has been shifted by 60° from that defined by Gubbels *et al.*[28] so that the coordinate systems defining the two PESs are the same; the angular coordinates for both PESs are defined as those described below Eq. (1).

We see for both PESs that there is a strong 3-fold corrugation with respect to the azimuthal angle ϕ (vertical direction in Fig. 2), corresponding to approach of the atom in a direction perpendicular to the C_3 axis, due to repulsion of the He atom by the D atoms. Since CD_3 is planar, the atom experiences the same interaction for approach both from above and below the molecular plane ($\theta < 90°$ and $\theta > 90°$, respectively). We see from Figs. 2(c) and 2(d) that approach of the atom toward the ND_3 lone pair ($\theta = 0°$) is more repulsive than approach on the side containing the D atoms ($\theta = 180°$). While the equilibrium geometry of ND_3 is nonplanar and hence the potential for approach of the atom from above and below the molecule is different, both the ± inversion vibrational wave functions have equal probability for the D atoms to be pointing up and down. We discuss below the parts of the ND_3–He PES responsible for collisions that conserve and change the ± inversion level.

The angular expansion of the PES given in Eq. (1) simplifies the calculation of matrix elements of the interaction potential between channel basis functions. We expect that the transitions with the largest cross sections will be those for which there is direct coupling through the larger angular expansion coefficients $V\lambda\mu$. Since CD_3 is planar and has a C_3 rotational symmetry axis, the only nonzero $V\lambda\mu$ terms are those for which $\lambda + \mu$ is even and μ is a multiple of 3. In the two-state model describing the ND_3 inversion motion, the even $\lambda + \mu$ terms enable inelastic transitions conserving the ± inversion quantum number, while odd $\lambda + \mu$ terms control inversion-changing transitions.[11] As with CD_3–He, the nonzero $V\lambda\mu$ terms for ND_3–He must have μ a multiple of 3.

Since we are comparing inelastic scattering dynamics of noninverting CD_3 and inverting ND_3, we will concentrate below on collision-induced transitions in ND_3 that conserve the ± inversion quantum number. Figure 3 compares the larger angular expansion coefficients $V\lambda\mu(R)$ for CD_3–He and ND_3–He for which $\lambda + \mu$ is even. The isotropic V_{00} term is comparable in magnitude for both systems. We also see that the largest anisotropic terms for both systems are V_{33} and then V_{20}, and that these are comparable in magnitude or larger than the isotropic term for values of R smaller than that of the global minima. The sign of the V_{20} term is different for the two systems; this is discussed below.

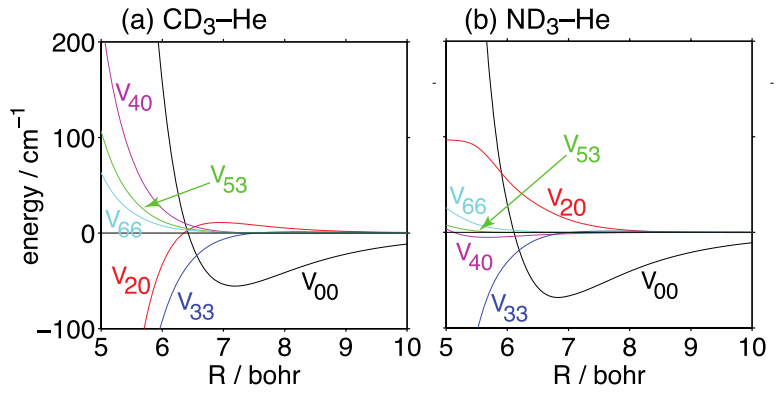

FIG. 3. Dependence of the larger even $\lambda + \mu$ expansion coefficients $V\lambda\mu(R)$ [defined in Eq. (1)] upon the atom-molecule separation R for (a) CD_3–He and (b) ND_3–He.

As we discussed in the Introduction, there are two types of anisotropies in the PES for the interaction of an atom with a nonlinear polyatomic molecule. To visualize the anisotropy upon approach of the atom around the molecular C_3 symmetry axis, we plot in Figs. 4(a) and 4(c) respectively the dependence of the interaction energy upon the azimuthal angle ϕ for $\theta = 90°$ of

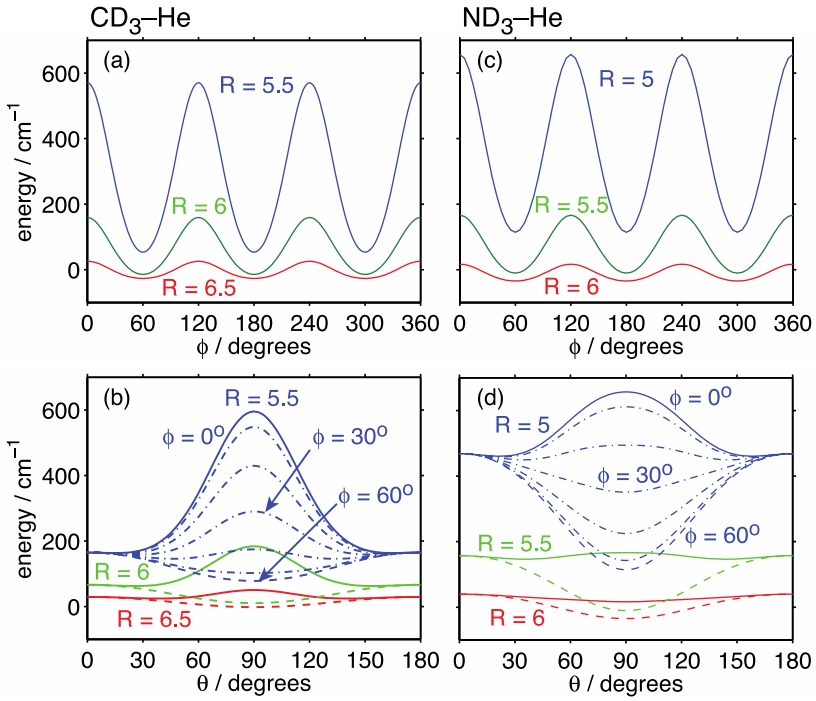

FIG. 4. Dependence of the interaction potential energy, computed from the larger even $\lambda + \mu$ expansion coefficients $V\lambda\mu(R)$ [defined in eqn 1], upon the atom-molecule separation R (in bohr) for (a) and (b) CD_3–He and (c) and (d) ND_3–He. The panels (a) and (c) show plots of azimuthal anisotropy at fixed $\theta = 90°$ and (b) and (d) as polar anisotropy at $\phi = 0°$ (solid lines) and $60°$ (dashed lines), respectively.

the CD_3–He PES and the part of the ND_3–He PES that governs ± inversion conserving transitions (even $\lambda + \mu$ terms) for several values of R. We see that the corrugation for small R is greater for CD_3–He than for ND_3–He, consistent with the larger equilibrium atom-molecule separation for the former. For both systems, the maximum repulsion occurs at $\phi = 0°$, 120°, and 240° for $\theta = 90°$. This ϕ dependence arises largely from the V_{33} term. From Eq. (1), the term multiplying V_{33} is proportional to $-\sin^3\theta\cos 3\phi$. The product of this term and a negative V_{33} has maxima at the same values of ϕ.

To visualize the dependence of the interaction energy for approach of the atom along *vs.* perpendicular to the symmetry axis, we plot in Figs. 4(b) and 4(d) the dependence of the CD_3–He PES and the even $\lambda + \mu$ part of the ND_3–He PES upon θ for several values of R and the azimuthal angle ϕ. For both systems the repulsion depends strongly upon ϕ at small R; for the smallest value of R in both plots the interaction energy is plotted for ϕ = 0°–60° (which correspond to approach of He along a C/N–D bond and between two bonds, respectively) in 10° increments. For the smallest value of R the repulsion in the ND_3–He system is seen to be the greater at $\theta = 90°$ than at $\theta = 0°/180°$ for most values of ϕ, while the opposite is true for CD_3–He. For both systems, the θ dependence is well described by the V_{20} term (with positive and negative values for CD_3–He and ND_3–He, respectively), which from Eq. (1) contains $(3\cos^2\theta - 1)/2$ in the angular expansion of the potential. This is due to the fact that the repulsion due to the nitrogen lone pair on ND_3 is greater than that due to the singly occupied out-of-plane 2*p* orbital on CD_3. We see from Fig. 4 that for both systems the anisotropy for approach of the atom around the symmetry axis (*e.g.* through the V_{33} term) is greater than the anisotropy for approach of the atom along or perpendicular to the symmetry axis (*e.g.* through the V_{20} term).

The $V_{\lambda\mu}$ terms with $\mu \neq 0$ for both CD_3–He and ND_3–He directly couple rotational levels differing by a multiple of 3 in the body-frame projection quantum number. Hence, the V_{33} term couples levels with k differing by ±3. Since rotational wave-functions of definite symmetry have ± signed-k components [see Eq. (12) of Ref. 30 or Eq. (4) of Ref. 27], the signed $k = \pm 1$ components of $k = 1$ levels of E nuclear symmetry are directly coupled to the signed $k = \mp 2$ components of $k = 2$ levels by the V_{33} term. We also note that a $V_{\lambda\mu}$ term can directly couple rotational levels for which the change Δn of the rotational angular momentum is less than or equal to λ. The $\mu = 0$ terms (*e.g.* the V_{20} term) enable Δn transitions within a given k manifold.

C. Quantum scattering calculations

The HIBRIDON suite of programs[32] and a separate scattering code written in Nijmegen were used to carry out quantum close-coupled scattering calculations to compute state-resolved integral and differential cross sections for collisions of CD_3 and ND_3 with He, respectively. Rotational energies were computed with a rigid rotor symmetric top Hamiltonian using spectroscopic parameters from Sears *et al.*[33] for CD_3. The methyl radical is an open-shell species, with doublet spin multiplicity, so that each rotational level, with rotational angular momentum n, is split into spin doublets, with total angular momentum $j = n \pm 1/2$. We have ignored spin in our scattering calculations since the spin-rotation and hyperfine splittings are small[34] and not resolved in our REMPI spectra. In the two-state model for ND_3, rotational energies were computed with a rigid rotor symmetric top Hamiltonian using experimental values for the rotational constants[35] and the inversion splitting.[36] Separate calculations were carried out for each of the three nuclear spin modifications of CD_3 and ND_3 since they are not interconverted in collisions with closed-shell species without nuclear spin.

Convergence of the differential cross sections was checked with respect to the size of the rotational basis and the number of partial waves in the calculation. Rotational levels whose energies were less than 1100 cm^{-1} were included in the channel basis for the CD_3–He system, and the calculations included total angular momenta $J \leq 130\ \hbar$. For ND_3, all rotational levels up to $n = 10$ (560 cm^{-1}) were included in the channel basis and all partial wave contributions up to $J = 100\ \hbar$ were taken into account.

III. Results and Discussion

A. Integral cross sections

The effect of the two types of anisotropy in the CD_3–He PES can be clearly seen in the state-to-state integral cross sections out of the lowest CD_3 rotational levels of each nuclear spin symmetry at a collision energy of 440 cm^{-1}, corresponding to the collision energy in the molecular beam experiment.[1] Figure 5 presents computed integral cross sections for transitions out of the 0_0 (A_2 nuclear spin symmetry), 1_0 (A_1 symmetry), and 1_1 (E symmetry) levels. For the 0_0 and 1_0 initial levels, the largest cross section is found for the transition to the 3_3 final level. These initial and final levels are coupled by the large V_{33} term. In addition, the transitions to the 6_6 final levels also have substantial cross sections; these are enabled either by direct

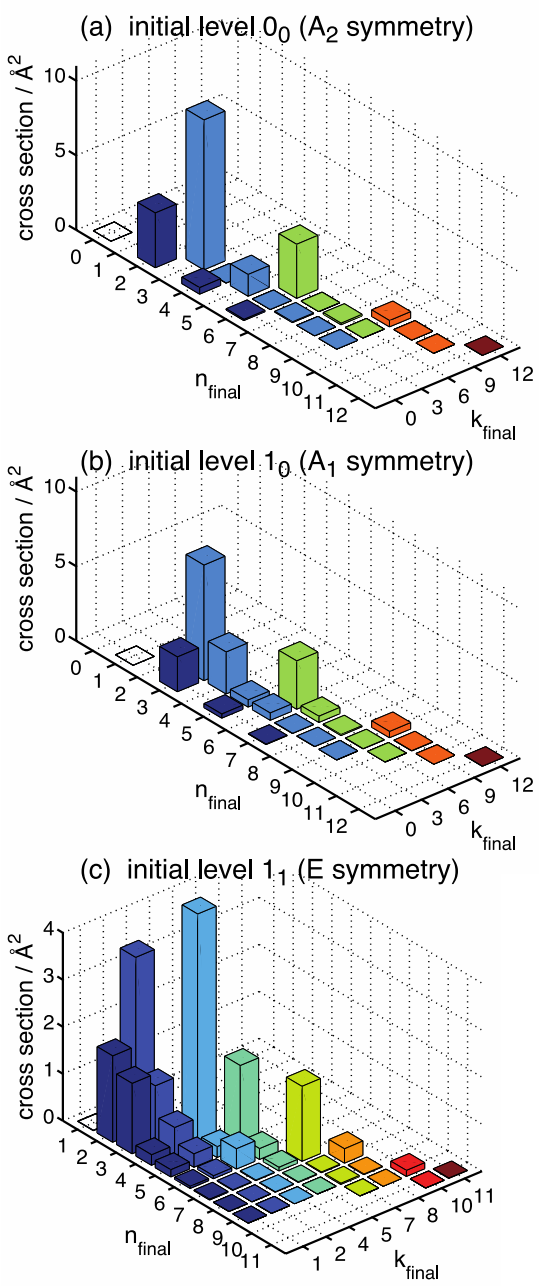

FIG. 5. Integral cross sections for transitions out of the lowest CD_3 levels of each nuclear spin symmetry at a relative translational energy of 440 cm^{-1} in collisions with helium. The initial levels are indicated with open squares.

coupling of the V_{66} term, or second-order transitions involving the V_{33} term. We see that the cross sections for transitions within the $k = 0$ manifold, which are enabled by the V_{20} and other $\mu = 0$ terms, are significantly smaller. This is consistent with the smaller magnitude of the V_{20} term as compared with the V_{33} term (see Fig. 3).

For the CD_3 1_1 initial level, the largest cross sections involve transitions to the 2_2 and 4_4 levels. Both of these final levels are directly coupled to the initial level by the V_{33} term, as discussed at the end of Sec. II.B. Other reasonably strong $k \neq 0$ transitions access the 5_5 and 7_7 final levels. These levels can be directly coupled to the initial level through the V_{66} term, or second-order transitions involving the V_{33} term. Propensities in state-to-state integral cross sections for collisions of higher CH_3 rotational levels of E symmetry with helium are discussed in Ref. 27.

The lowest-energy ND_3 rotational levels of A_1, A_2, and E nuclear spin symmetry are the 0_0^+, 0_0^- and, 1_1^+ levels, respectively. The cross sections for transitions out of the 0_0^+ and 0_0^- levels conserving the ± inversion level are virtually identical, and likewise for transitions changing the inversion level, since the coupling matrix elements are the same but the energies of inversion levels are slightly different.[37] We hence present in Fig. 6 state-to-state integral cross

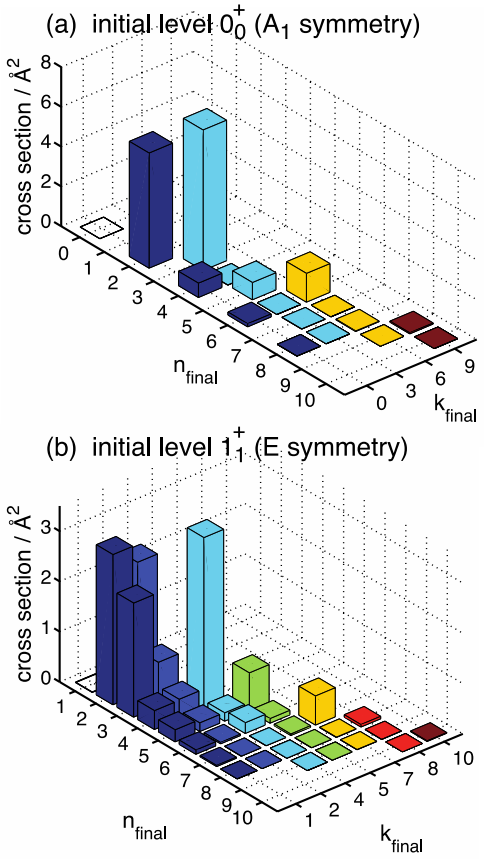

FIG. 6. Integral cross sections for transitions out of the lowest ND_3 levels of each nuclear spin symmetry at a relative translational energy of 430 cm^{-1} in collisions with helium. The initial levels are indicated with open squares.

sections for inversion conserving transitions out of the ND_3 rotational 0_0^+ and 1_1^+ levels at a collision energy of 430 cm^{-1}, corresponding to the collision energy in the molecular beam experiment.[2] We note in passing that the sum of the ICSs for the inversion changing transitions are ~28% of the sum of ICSs for the inversion conserving transitions for these initial levels. For both initial levels, the largest cross sections plotted in Fig. 6 are for Δk = +3 transitions, namely the $0_0^+ \rightarrow 3_3^+$ and $1_1^+ \rightarrow 4_4^+$ transitions, connected mainly through the V_{33} term. In contrast to the CD_3–He system, the largest cross sections for Δk = 0 transitions are comparable in magnitude to those for the Δk = +3 transitions. We also see that for the 1_1^+ initial level, cross sections for transitions to final levels with the k = 2 manifold are substantial in size. These transitions are also enabled by the strong V_{33} term.

The Δk = 0 transitions are the only transitions that have systematically larger ICSs for the ND_3 – He system conserving ± symmetry than for the CD_3–He system (with the exception of the $0_0 \rightarrow 4_3$ and 7_6 transitions, which are not directly coupled by any of the expansion coefficients discussed above). The larger ICSs for the ND_3–He system for transitions enabled by $V_{\lambda 0}$ terms are caused by the stronger anisotropy in the θ coordinate [see Fig. 4(b) vs. Fig. 4(d)]. Integral cross sections for transitions enabled by $V_{\lambda 0}$ and V_{33} terms out of the lowest ND_3 and CD_3 levels of each nuclear spin symmetry at a relative translational energy of 430 cm^{-1} in collisions with helium are shown in Fig. 7. In the next subsection we discuss trends in the differential state-to-state cross sections while we keep in mind the magnitude of the corresponding integral cross sections.

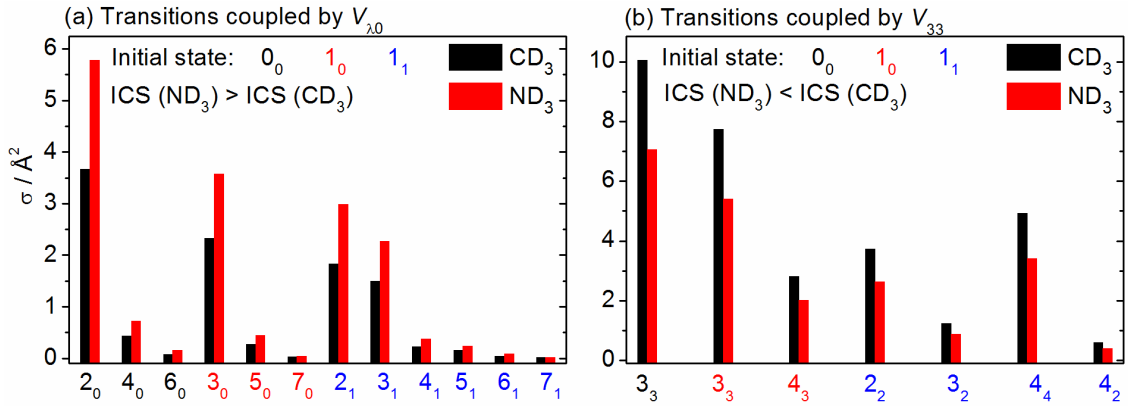

FIG. 7. Integral cross sections for transitions enabled by (a) $V_{\lambda 0}$ and (b) V_{33} terms out of the lowest ND_3 and CD_3 levels of each nuclear spin symmetry at a relative translational energy of 430 cm^{-1} in collisions with helium. The initial levels are indicated with color coding.

B. Differential cross sections

Direct comparison of experimentally determined DCSs for inelastic scattering of ND_3 and CD_3 with He is not possible for most of the final levels, because the CD_3 REMPI lines are not resolved in the k projection quantum number.[1] The only measured k–resolved line for CD_3 corresponds to detection of the 2_1 final level. The experimental DCSs for inelastic scattering of CD_3 into $n'_{k'} = 2_1$ and ND_3 into 2_1^- and 2_1^+ levels from the 1_1 and 1_1^- levels, respectively, in collision with He are compared in Fig. 8. The DCS for CD_3 is normalized to match the value at $\theta = 30°$ with that for ND_3 (2_1^-), whereas the DCS for ND_3 (2_1^+) is normalized to match the DCS for ND_3 (2_1^-) at $\theta = 150°$. In the experiments, the ND_3 was prepared in a single initial state 1_1^-, whereas the CD_3 initially populated several levels, the most significant of which is 1_1. The DCS for CD_3 scattering agrees well with that for ND_3 (2_1^-), whereas the inversion-symmetry changing DCS for ND_3 (2_1^+) differs from both.

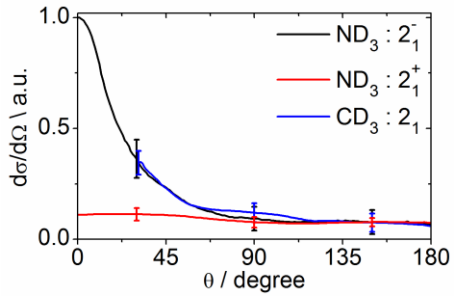

FIG. 8. Comparison of the experimental DCSs for inelastic scattering of CD_3 into the $n'_{k'} = 2_1$ level and ND_3 into the 2_1^- and 2_1^+ levels from the 1_1 and 1_1^- initial levels, respectively, in collisions with He. The methods of normalization of the data are described in the main text.

Figure 9 shows a comparison of calculated DCSs for the ND_3–He and CD_3–He systems for the E nuclear spin modification for transitions to five low lying final levels (see Fig. 1). The DCSs for CD_3–He were calculated for the $n_k = 1_1$ initial level, whereas the DCSs for ND_3–He are plotted for both 1_1^- and 1_1^+ initial levels and $n'^-_{k'}$ final levels. We note that for the ND_3–He system the n_k^- to $n'^-_{k'}$ and n_k^+ to $n'^+_{k'}$ transitions have essentially identical DCSs, and therefore we show only DCSs for – inversion symmetry.[2] The DCSs were calculated at a collision energy of 440 cm^{-1} for CD_3–He and 430 cm^{-1} for ND_3–He, which correspond to the experimental collision energies. The small difference in collision energies will have a negligible effect on the DCSs, as shown in supplementary information of the recent ND_3–He paper.[2] In this section, we show only a representative sample of DCSs for both systems. Further comparisons of computed DCSs

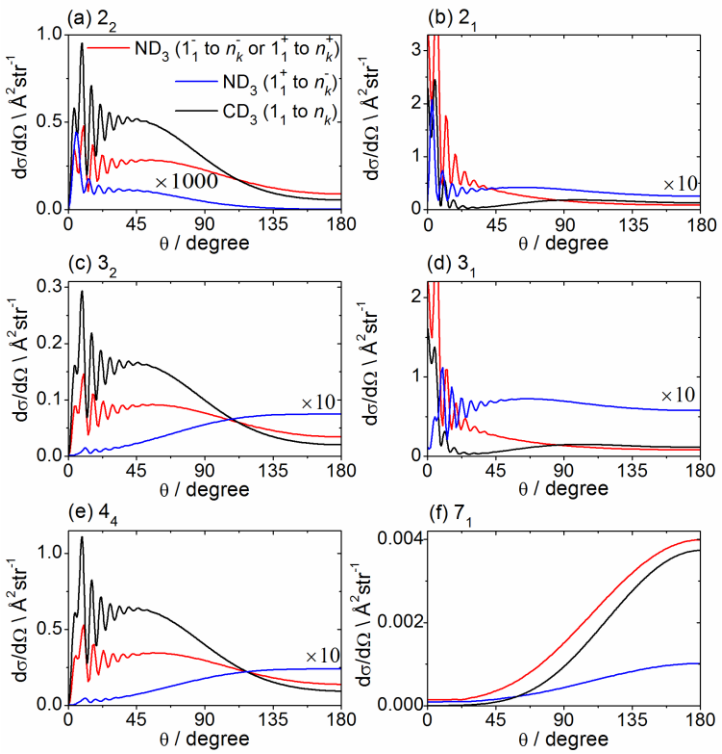

FIG. 9. Comparison of the theoretical DCSs for inelastic scattering of CD_3 (1_1 to $n'_{k'}$ transitions) with He at a collision energy of 440 cm^{-1} (black lines) and ND_3 with He (1_1^- to $n'^-_{k'}$ or 1_1^+ to $n'^+_{k'}$ transitions, which are identical) at a collision energy of 430 cm^{-1} (red lines). The DCSs for ND_3 scattering with He for the 1_1^+ to $n'^-_{k'}$ transition (blue lines) are also plotted, and have been vertically scaled as indicated for ease of comparison.

for transitions out of the lowest rotational levels of each nuclear spin modification can be found online from EPAPS.[38]

The DCSs for scattering into these low lying final levels for CD_3–He resemble the DCSs for ND_3–He that conserve the ± inversion symmetry in the collision, whereas the scattering dynamics for ± symmetry changing collisions differ. The ± symmetry conserving transitions in ND_3 are enabled by the same expansion coefficients $V\lambda\mu$ as in CD_3 scattering dynamics (with $\lambda + \mu$ even, in contrast to ± symmetry changing transitions where $\lambda + \mu$ is odd). This differing behaviour for ± symmetry conserving *vs.* changing transitions is especially evident for the 3_2 and 4_4 final levels of ND_3 [see Figs. 9(c) and 9(e)]. The magnitudes (and hence integral cross sections) for ± symmetry changing collisions are much lower, and these DCSs were therefore multiplied by a constant scaling factor to be visible in Fig. 9.

Although there are many similarities between the DCSs for ND_3–He and CD_3–He scattering, observed differences can be linked to $V_{\lambda\mu}$ terms which directly couple given transitions. The transitions directly coupled by terms other than the large V_{20} and V_{33} terms could be enabled by higher-order transitions involving these large terms. For example, transitions directly coupled by the V_{66} or V_{53} terms can also be enabled by transitions involving the V_{33} term twice or a combination of V_{33} and V_{20} terms, respectively.

We see that the DCSs for scattering of CD_3 into the 2_2, 3_2, and 4_4 final levels and the corresponding ND_3 transitions conserving the inversion symmetry have a similar shape. These transitions, which are coupled directly by the V_{33} term, all display broad DCSs, starting from zero intensity at $\theta = 0°$ and extending over the entire angular range, with oscillations at small angles ($\theta \leq 45°$). The DCS for CD_3 is always more forward scattered than the corresponding DCS for ND_3 for transitions dominated by the V_{33} term in the potential. The similarity in DCSs for transitions directly coupled by the V_{33} term for the two systems reflects the similarity of V_{33} in both the radial dependence and magnitude [see Figs. 3, 4(a), and 4(c)]. The partial cross sections for CD_3–He and ND_3–He collisions involving the $1_1 \rightarrow 3_2$ transition conserving and changing the inversion symmetry are shown in Fig. 10. The scattering occurs over similar ranges of total angular momentum (classically over similar impact parameters) for CD_3 and ND_3 conserving inversion symmetry, whereas the scattering leading to a change of the inversion symmetry occurs on average at smaller impact parameters, and these collisions result in a backward peaking DCS.

By contrast, there are significant differences in the CD_3 and ND_3 (conserving inversion symmetry) DCSs for transitions into the 2_1 and 3_1 levels plotted in Fig. 9, which are enabled by direct coupling through the V_{20} term. The DCSs for the CD_3–He system exhibit a dip in the forward hemisphere around $\theta = 25°$, whereas for ND_3–He the DCSs continuously rise and peak in the forward hemisphere. The partial cross sections for the $1_1 \rightarrow 2_1$ transition for CD_3–He and ND_3–He collisions conserving and changing the inversion symmetry are shown in Fig. 10(b). We see a dip in the CD_3–He partial cross sections around $J = 27$ ($b = 5.8$ bohr), while the ND_3–He partial cross section decreases monotonically with increasing J from its maximum value.

The $\Delta k = 0$ transitions, which are directly coupled by the expansion coefficients with $\mu = 0$ ($V_{\lambda 0}$), are shown in panels b, d, and f of Fig. 9. These expansion coefficients with $\mu = 0$ describe the anisotropy in the θ coordinate.[27] The differences in the DCSs for small Δn transitions [in Figs. 9(b) and 9(d)] are a manifestation of the difference in the V_{20} terms for the systems of

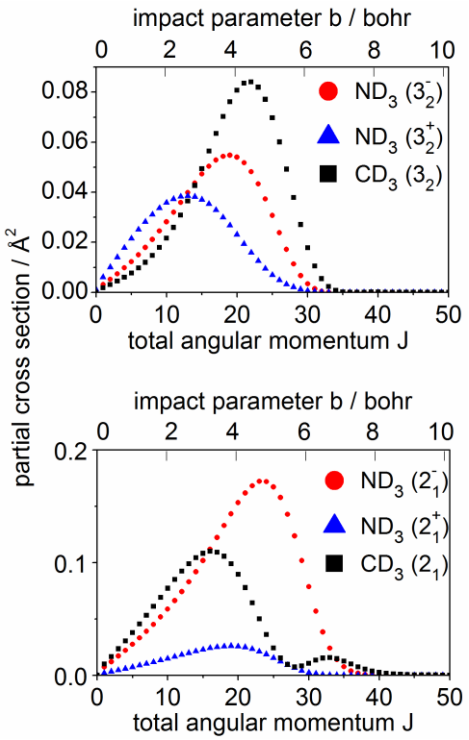

FIG. 10. Partial cross sections for CD_3–He and ND_3–He systems at a collision energy 440 cm^{-1} for scattering from the 1_1 and 1_1^- initial levels into (a) 2_1 and (b) 3_2 final levels (with both inversion symmetries for ND_3).

interest [see Figs. 3, 4(b) and 4(d)]. On the other hand, the ND_3–He and CD_3–He DCSs for Δk = 0 transitions for large Δn are very similar except for the absolute value, as can be seen in Fig. 9(f).

The DCSs for transitions directly coupled by the V_{66} term are completely backward scattered for ND_3 with maxima at θ = 180°, whereas they exhibit maxima at intermediate scattering angles (θ = 110 – 135°) for CD_3. Examples of DCSs enabled by the V_{66} term are shown for CD_3 and ND_3 in Fig. 11(a) for the 1_1 to 5_5 transition. The maxima of the DCSs for CD_3 shift to larger scattering angles as the amount of transferred energy associated with the transition increases.

The transitions directly coupled by the V_{53} term exhibit completely backward scattered DCSs with maxima at θ = 180° for CD_3, and DCSs dominated by sideways scattering for ND_3 with maxima typically at intermediate scattering angles. This behaviour is opposite to that seen for the transitions directly coupled by the V_{66} term. Examples of DCSs for both systems directly coupled by the V_{53} term are shown in Fig. 11(b) for the 1_0 to 5_3 transition. The maxima of the

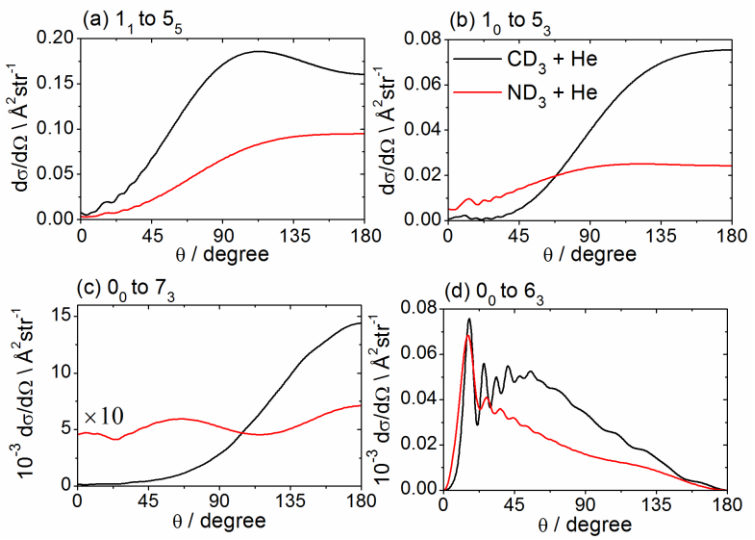

FIG. 11. Comparison of the theoretical DCSs for inelastic scattering of CD_3 with He at a collision energy of 440 cm^{-1} (black lines) and ND_3 with He at a collision energy of 430 cm^{-1} (red lines) for a selection of transitions.

DCSs for ND_3 move to larger scattering angles as the internal energy change in a collision increases. Whereas the transitions in CD_3 directly coupled by the V_{73} term are associated with backward scattering, the DCSs for ND_3 exhibit oscillatory behaviour as illustrated in Fig. 11(c) for the 0_0 to 7_3 transition. The V_{73} term is very weak in comparison with other expansion coefficients and therefore not shown in Fig. 3. The transitions directly coupled by this term will be enabled mainly by a combination of larger expansion coefficients through multiple quantum transitions. These transitions for ND_3 are very weak and the example DCS had to be multiplied by 10 to be visible. For the transitions controlled by the V_{53} and V_{73} terms, and associated with the largest internal energy changes ($1_0 \rightarrow 6_3$ and $1_1 \rightarrow 6_2$), the scattering maxima shift to θ = 180°.

Some transitions (e.g., $0_0 \rightarrow 4_3$, 6_3, 7_6) are not directly coupled by any of the large expansion coefficients and they are enabled only by a combination of the expansion coefficients through the multiple-order transitions. By way of example, Fig. 11(d) shows DCSs for ND_3 and CD_3 for the $0_0 \rightarrow 6_3$ transition. The DCSs are similar for both systems and the ICSs are much smaller than for directly coupled transitions. Note that the DCSs are dominated by diffraction oscillations at small angles, even though the DCSs for transitions associated with approximately the same amount of energy transfer, but directly coupled by expansion coefficients of the

potential, do not exhibit such oscillations. For the systems of interest, they are present only for transitions into final levels with $n' \leq 4$.

The initial to final rotational level transitions can also be directly coupled by more than one of the expansion coefficients. For example, $1_1 \rightarrow 4_4$ and 4_2 are both directly coupled by the V_{33} and V_{53} terms. These DCSs are shown in Fig. 12 for CD_3 as well as for ND_3. The $1_1 \rightarrow 4_4$ transition has a broad peak characteristic of DCSs enabled solely by the V_{33} term, whereas the DCSs for the $1_1 \rightarrow 4_2$ transition resemble those expected for transitions enabled solely by the V_{53} term.

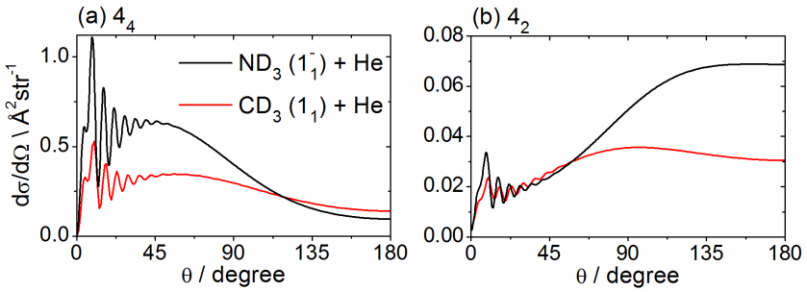

FIG. 12. Comparison of the theoretical DCSs for inelastic scattering of CD_3 with He at a collision energy of 440 cm^{-1} (black lines) and ND_3 with He at a collision energy of 430 cm^{-1} (red lines) for (a) $1_1 \rightarrow 4_4$ and (b) $1_1 \rightarrow 4_2$ transitions directly coupled by the V_{33} and V_{53} terms.

IV. Conclusions

We have presented a comparison of the scattering dynamics of two deuterated symmetric top molecules, one closed-shell (ND_3) and the other an open-shell radical (CD_3) in collisions with He. The scattering dynamics are compared on the basis of close-coupling quantum-mechanical scattering calculations that used *ab initio* PESs. These theoretical studies were carefully validated by comparison to experimental measurements of rotationally resolved differential cross sections, as described in two recent publications.[1,2] The comparisons drawn here are between the inelastic scattering dynamics of non-inverting CD_3 and umbrella-motion inverting ND_3, and so concentrate on collision-induced transitions in ND_3 that conserve the ± inversion symmetry.

The transitions with the largest ICSs are those for which there is direct coupling through the larger angular expansion coefficients $V_{\lambda\mu}$ of the PES. For the interaction of an atom with a nonlinear polyatomic molecule, two types of anisotropy influence the scattering dynamics. For

both systems the anisotropy in the ϕ coordinate (described predominantly by the V_{33} term in an expansion of the potential in angular functions) is greater than the anisotropy in the θ coordinate (described by the V_{20} term). The isotropic V_{00} term is comparable in magnitude for both systems. The largest anisotropic terms for both systems are V_{33} and V_{20}, and these are comparable in magnitude or larger than the isotropic contribution to the potential for values of R smaller than those of the global minima. However, the signs of the V_{20} terms are different (at small values of R) for the two scattering systems. The differences in integral and state-resolved differential cross sections for rotationally inelastic scattering of CD_3 and ND_3 with He reflect the differences in magnitude and effect of individual expansion coefficients of the potential. The effect of the two anisotropies is clearly seen in the state-to-state integral cross sections out of the lowest CD_3 rotational levels of each nuclear spin symmetry at a collision energy of 440 cm^{-1}: the ICSs coupled by the V_{33} term are larger than ICSs enabled by the V_{20} term. The $\Delta k = 0$ transitions are the only transitions that have systematically larger ICSs for the ND_3–He system conserving ± symmetry than for the CD_3–He system (with the exception of the $0_0 \rightarrow 4_3$ and 7_6 transitions, which are not directly coupled by any of the expansion coefficients). The larger ICSs for the ND_3–He system for transitions enabled by $V_{\lambda 0}$ terms are caused by the stronger anisotropy in the θ coordinate.

There are many similarities between the DCSs for ND_3–He (conserving ± symmetry) and CD_3–He scattering, nevertheless observed differences can be linked to $V_{\lambda\mu}$ terms which directly couple given transitions. The transitions directly coupled by the V_{33} term display broad DCSs starting from zero intensity at $\theta = 0°$ and extending over the entire angular range for both systems. In this case, the DCS for CD_3 is always more forward scattered than the corresponding DCS for ND_3. The similarity in DCSs for transitions directly coupled by the V_{33} term for the two systems reflects the similarity of V_{33} in both the radial dependence and magnitude. In addition the scattering occurs over similar ranges of total angular momentum (classically over similar impact parameters) for CD_3 and ND_3 (conserving inversion symmetry). The $\Delta k = 0$ transitions directly coupled by the $V_{\lambda 0}$ expansion coefficients exhibit differences in the DCSs for small Δn transitions, which reflects the difference in the V_{20} terms for the systems. On the other hand, the DCSs for large Δn transitions are very similar. These expansion coefficients with $\mu = 0$ describe the anisotropy in the θ coordinate.

Acknowledgements

The Bristol group acknowledges financial support from the EPSRC Programme Grant EP/G00224X. The theoretical work by P.J.D. and M.H.A. was supported by the Chemical, Geosciences and Biosciences Division, Office of Basic Energy Sciences, Office of Science, U.S. Department of Energy, under Grant No. DESC0002323. The Bristol group is part of the EU Marie Curie Initial Training Network *ICONIC* which provided financial support for O.T.

References

1. O. Tkáč, A. K. Sage , S. J. Greaves, A. J. Orr-Ewing, P. J. Dagdigian, Q. Ma, and M. H. Alexander, Chem. Sci. **4**, 4199 (2013).
2. O. Tkac, A. K. Saha, J. Onvlee, C.-H. Yang, G. Sarma, C. K. Bishwakarma, S. Y. T. van de Meerakker, A. van der Avoird, D. H. Parker, and A. J. Orr-Ewing, Phys. Chem. Chem. Phys. **16**, 477 (2014).
3. F. J. Aoiz, J. E. Verdasco, M. Brouard, J. Kłos, S. Marinakis, and S. Stolte, J. Phys. Chem. A **113**, 14636 (2009).
4. C. J. Eyles, M. Brouard, H. Chadwick, F. J. Aoiz, J. Kłos, A. Gijsbertsen, X. Zhang, and S. Stolte, Phys. Chem. Chem. Phys. **14**, 5420 (2012).
5. C. J. Eyles, M. Brouard, H. Chadwick, B. Hornung, B. Nichols, C. H. Yang, J. Kłos, F. J. Aoiz, A. Gijsbertsen, A. E. Wiskerke, and S. Stolte, Phys. Chem. Chem. Phys. **14**, 5403 (2012).
6. C. J. Eyles, M. Brouard, C. H. Yang, J. Kłos, F. J. Aoiz, A. Gijsbertsen, A. E. Wiskerke, and S. Stolte, Nature Chem. **3**, 597 (2011).
7. S. Antonova, A. Lin, A. P. Tsakotellis, and G. C. McBane, J. Chem. Phys. **110**, 11742 (1999).
8. A. Gijsbertsen, H. Linnartz, G. Rus, A. E. Wiskerke, S. Stolte, D. W. Chandler, and J. Klos, J. Chem. Phys. **123**, (2005).
9. G. Sarma, S. Marinakis, J. J. ter Meulen, D. H. Parker, and K. G. McKendrick, Nature Chem. **4**, 985 (2012).
10. E. A. Wade, K. T. Lorenz, J. L. Springfield, and D. W. Chandler, J. Phys. Chem. A **107**, 4976 (2003).
11. S. Green, J. Phys. Chem. **73**, 2740 (1980).
12. T. R. Phillips, S. Maluendes, and S. Green, J. Chem. Phys. **102**, 6024 (1995).
13. J. Schleipen, J. J. ter Meulen, G. C. M. van der sanden, P. E. S. Wormer, and A. van der Avoird, Chemical Physics **163**, 161 (1992).
14. J. Schleipen, J. J. ter Meulen, and A. R. Offer, Chemical Physics **171**, 347 (1993).
15. W. B. Chapman, A. Schiffman, J. M. Hutson, and D. J. Nesbitt, J. Chem. Phys. **105**, 3497 (1996).

16. W. B. Chapman, A. Kulcke, B. W. Blackmon, and D. J. Nesbitt, J. Chem. Phys. **110**, 8543 (1999).
17. C. H. Yang, G. Sarma, J. J. ter Meulen, D. H. Parker, U. Buck, and L. Wiesenfeld, J. Phys. Chem. A **114**, 9886 (2010).
18. C. H. Yang, G. Sarma, D. H. Parker, J. J. ter Meulen, and L. Wiesenfeld, J. Chem. Phys. **134**, 204308 (2011).
19. L. Ma, M. H. Alexander, and P. J. Dagdigian, J. Chem. Phys. **134**, 154307 (2011).
20. L. Ma, P. J. Dagdigian, and M. H. Alexander, J. Chem. Phys. **136**, 224306 (2012).
21. L. Wiesenfeld and A. Faure, Mon. Not. R. Astron. Soc. **432**, 2573 (2013).
22. P. J. Dagdigian, Int. Rev. Phys. Chem. **32**, 229 (2013).
23. M. N. R. Ashfold, S. R. Langford, R. A. Morgan, A. J. Orr-Ewing, C. M. Western, C. R. Scheper, and C. A. de Lange, Eur. Phys. J. D **4**, 189 (1998).
24. L. Fusina and S. N. Murzin, J. Mol. Spectr. **167**, 464 (1994).
25. C. Leonard, S. Carter, and N. C. Handy, Chem. Phys. Lett. **370**, 360 (2003).
26. G. Herzberg, *Molecular Spectra and Molecular Structure III. Electronic Spectra and Electronic Structure of Polyatomic Molecules* (D. Van Nostrand, Princeton, NJ, 1967).
27. P. J. Dagdigian and M. H. Alexander, J. Chem. Phys. **135**, 064306 (2011).
28. K. B. Gubbels, S. Y. T. van de Meerakker, G. C. Groenenboom, G. Meijer, and A. van der Avoird, J. Phys. Chem. **136**, (2012).
29. Q. Ma, P. J. Dagdigian, and M. H. Alexander, J. Chem. Phys. **138**, 104317 (2013).
30. S. Green, J. Phys. Chem. **64**, 3463 (1976).
31. J. Millan, N. Halberstadt, G. C. M. van der Sanden, and A. van der Avoird, J. Phys. Chem. **103**, 4138 (1995).
32. HIBRIDON is a package of programs for the time-independent quantum treatment of inelastic collisions and photodissociation written by M. H. Alexander, D. E. Manolopoulos, H.-J. Werner, B. Follmeg, P. J. Dagdigian, Q. Ma, and others. More information and/or a copy of the code can be obtained from the website http://www2.chem.umd.edu/groups/physical/hibridon/hib43.
33. T. J. Sears, J. M. Frye, V. Spirko, and W. P. Kraemer, J. Chem. Phys. **90**, 2125 (1989).
34. S. Davis, D. T. Anderson, G. Duxbury, and D. J. Nesbitt, J. Chem. Phys. **107**, 5661 (1997).
35. M. Snels, L. Fusina, H. Hollenstein, and M. Quack, Mol. Phys. **98**, 837 (2000).

36. J. van Veldhoven, R. T. Jongma, B. Sartakov, W. A. Bongers, and G. Meijer, Phys. Rev. A **66**, (2002).
37. S. L. Davis and J. E. Boggs, J. Phys. Chem. **69**, 2355 (1978).
38. See Supplementary Material Document No._____ for computed DCSs of transitions out of the lowest rotational levels of each nuclear spin modification. For information on Supplementary Material, see http://www.aip.org/pubservs/epaps.html.